Euroasia Journal of Mathematics, Engineering, Natural & Medical Sciences
International Indexed and Refereed
ISSN 2667-6702

The Design and Control of a New Lower Limb Rehabilitation Robot for Active and Active-assisted Exercises

Aktif ve Aktif Yardımlı Rehabilitasyon Egzersizleri için yeni bir Alt Ekstremite Rehabilitasyon Robotunun Tasarımı ve Kontrolü

Merve Teke Budaklı*

Dr., Turkish-German University, Faculty of Engineering, Department of Mecatronics Engineering, Istanbul, Türkiye

Cuneyt Yılmaz

Assoc. Prof. Dr., Yildiz Technical University, Faculty of Engineering, Department of Mecatronics, Istanbul, Türkiye

Faruk Bagcı

Prof. Dr., Turkish-German University, Faculty of Engineering, Department of Computer Science, Istanbul, Türkiye

** Corresponding author: tekebudakli@tau.edu.tr*

Geliş Tarihi / Received: 11.12.2023
Kabul Tarihi / Accepted: 24.12.2023

Araştırma Makalesi/Research Article
DOI: 10.5281/zenodo.10445926

ABSTRACT

The high position accuracy and rigidity of robots are very important in interventions to the human body. Due to its closed chain kinematic structure, parallel robots exhibit superior positioning accuracy and rigid body structure. Although these reasons lead to the preference of rehabilitation robots, the closed chain kinematic structure introduces a limited working space which restricts the robot to perform the necessary rehabilitation exercises through one joint, solely. Based on this fact, a newly constructed rehabilitation robot ensuring the same positioning accuracy of a parallel robot and also an increased working space has been utilized in this work. This rehabilitation robot represents a parallel robot as a Stewart Platform structure including a 7^{th} linear actuator combined with a trajectory stabilizer. By means of its expanded working space, this robot system offers the possibility of rehabilitation in the ankle with plantarflexion-dorsiflexion, eversion-inversion, adduction-abduction and in the knee joint with extension-flexion ROMs. On these joints, active and active-assisted ROM rehabilitation with position-based impedance control structure have been applied. Measurements performed on two healthy volunteers revealed that the robot's standard ROM values could be brought with a maximum deviation of 1.3%, with the force or torque occurring in the “0” or reverse direction.

Keywords: Lower extremity rehabilitation robot, parallel robot, position-based impedance control, active rehabilitation exercises, active-assisted rehabilitation exercises

1. INTRODUCTION

The use of robots in the field of health has started to become widespread with the development of technology. Rehabilitation exercises, which are of great importance to restore the physical functions of the affected external limbs of individuals, have an important place in the field of health. Due to the differences in the physical and biological structures of patients, the effects of the same disease may vary according to the individuals. For this reason, the strength and range of motion that the

physiotherapist will apply during the treatment varies from person to person. Therefore, it takes long time for the physiotherapist to gain practical skills and experience after education. In addition, repetitive physiotherapy movements cause occupational body deformations for physiotherapists. However, the inability to measure the recovery of the patient's limb fully and rationally is among some of the problems of traditional rehabilitation methodologies.

Different robotic systems have been developed and are being developed to reduce or completely prevent these problems. In the literature, it is seen that the parallel robot structure comes to the fore in the design of rehabilitation robots that provide range of motion (ROM) in three axis in the ankle. The main reasons are the rigid structure of parallel robots as well as motion repetition, positioning precision, and high degrees of freedom. However, due to the reduced working space of parallel robots, rehabilitation applications with parallel robots in the literature have been limited to the ankle joint (Ayas et al., 2018; Ayas & Altas, 2018; M. Dong et al., 2021; M. Girone et al., 2001; M. J. Girone et al., 1999; Jamwal & Hussain, 2016; Liu et al., 2006; Rakhodaei et al., 2016; Tsoi & Xie, 2008; C. Wang et al., 2013). Diaz et al. reviewed ankle rehabilitation robots as a separate group in their review article on rehabilitation robots (Díaz et al., 2011). It is observed in the literature that serial robots are generally preferred in wearable and fixed rehabilitation robots for knee rehabilitation. At these robots, either only knee rehabilitation was provided or studies were carried out on combined rehabilitation movements with ankle and/or knee (F. Dong et al., 2022). However, it has been determined that serial robots that provide knee and ankle rehabilitation have the ability to move only in one axis (plantarflexion-dorsiflexion) in the ankle (Chisholm et al., 2014; Feng et al., 2016; Mohanta et al., 2018; Shen et al., 2020). In addition, in the knee joint, the posterior parts of the condyles have a common rotation center passing through the anterior and posterior cruciate ligament attachments. The anterior parts do not have a single rotation center due to their different morphological structures and three-dimensional movements (Eckhoff et al., 2007; Esmer et al., 2011). In these serial robots, only the rotational axis is used in the knee axis, and therefore, they cannot compensate for the forward translational movement of the tibia on the femur due to the axis shift seen in knee extension. Peng et al. reported ROM between −2° and +85° in the knee rehabilitation robot they designed (Peng et al., 2016). Wang et al. performed knee rehabilitation studies in the range of −5° to +95° (D. Wang et al., 2009). Chisholm et al. reported an ROM of 0° to +70° for the knee and −15° to +30° for the ankle (Chisholm et al., 2014). Feng et al. performed knee rehabilitation exercises between −120° - 0° and ankle exercises between −15° and +30°.

However, it was observed that these studied ranges could not reach the average normal range of motion determined by AMA (American Medical Association) and AAOS (American Academy of Orthopaedic Surgeons). In our previous study (Budaklı & Yılmaz, 2021), we designed a new robot system that can meet flexion-extension ROMs in the knee, and plantarflexion-dorsiflexion, eversion-inversion, adduction-abduction ROMs in the ankle joint according to AAOS and AMA. Beside that, passive exercises were performed with PID control in this robotic system. In this study, the position based impedance control structure was added to the related robot and the results of active and active-assisted rehabilitation exercises were evaluated by performing tests on healthy volunteers.

2. SYSTEM DESCRIPTION

It is aimed that the designed rehabilitation robot will perform passive, active and active assisted ROM rehabilitation exercises by meeting the flexion-extension ROMs in the ankle in three axis (plantarflexion-dorsiflexion, eversion-inversion, adduction-abduction) and in the knee joint. Passive and active rehabilitation with a seven-axis robotic structure in total, with a six-degree-of-freedom

parallel robot with Stewart platform structure that can provide a three-axis range of motion in the ankle and perform the linear movement of the knee forward, and a linear axis with a unique mechanism included in this parallel robot structure to meet the knee extension movement. A system has been designed to assist the treatment process by providing exercises. The designed rehabilitation robot can provide treatment to more patient groups by applying rehabilitation to the two joints of the right and left lower extremities. The rehabilitation robot basically consists of workstation, electronic hardware and robot mechanism parts. The general structure of the robot is shown in Fig. 1.

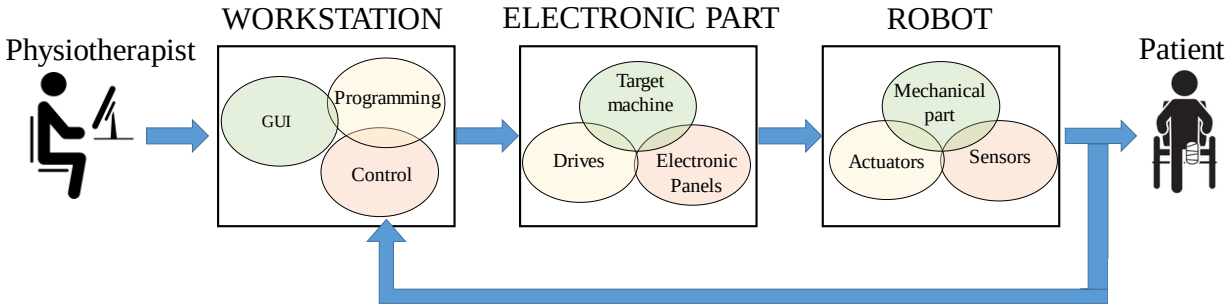

Fig. 1. General Structure of the Rehabilitation Robot.

The robot is designed to provide rehabilitation for individuals with a maximum weight of 180 kg and a heel-to-knee distance of 43 - 54 cm. The technical requirements and technical equipment of the rehabilitation robot in order to meet the relevant exercises and ROMs are given in Table 1.

Table 1. Technical Requirements and Equipments

Property	**Technical requirements**	**Technical equipments**
Maximum weight of the rehabilitated person: 180 kg	Actuator torque requirement: 400 N (6 pcs AC) 500 N (1 DC)	500 N (6 pcs AC) 800 N (1 DC)
Passive, active and assisted active exercises	Joint angle speed: 0.2 rad/s Engine speed: 30 mm/s	1 rad/s and 0,5 rad/s 150 mm/s (6 pcs AC) 80 mm/s (1 DC)
Required ROMs: x-axis: -20° - 30° y-axis: -20° - 40° z-axis: -10° - 20° Heel-to-knee distance: 43 - 54 cm	Stroke length: 200 mm (6 pcs AC) 300 mm (DC)	200 mm (6 pcs AC) 300 mm (DC)
Maximum force/torque exerted by the rehabilitated person	x-, y- axis: 150 N, ±10 z-axis: 400 N Torque= ±10 Nm	x-, y- axis: 165 N z-axis: 495 N Torque= ±15 Nm

The parallel robot provides both linear and rotational motion in the *x*, *y*, *z*-axis and has 6 degrees of freedom. However, the working space is not sufficient for the knee extension movement. A seventh linear actuator is incorporated into this parallel robot, which is designed to meet the ROMs required for knee rehabilitation.

Table 2. Mechanical Parts of Robot

Mechanical parts of parallel robot	Mechanical parts of additional mechanism
Upper plate	Movable foot plate
Fixed base plate	Trajectory stabilizer
Linear Actuator (6 pcs)	7th Linear actuator
Universal Joint (12 pcs)	Joints (2 pcs)
Mounting part (6 pcs)	Support unit for trajectory stabilizer

The design parts of both the parallel robot and the additional mechanism of the robot are shown in Table 2. The structure of the rehabilitation robot consists of the lower platform, the upper platform and 6 linear actuators with a stroke length of 200 mm between them (see Fig. 2). The linear actuators are fixed to the lower and upper platform with universal joints. In addition, inclined connectors made of steel material are mounted between the universal joints and the platforms. Thus, in the zero position, the universal joints are kept straight and can allow the upper platform to be tilted up to 50°. In knee extension movement, the parallel robot brings the knee up to a certain angle, then the seventh linear actuator engages and continues the movement for maximum extension ROM. In this case, only the 7th linear actuator needs to leave the platform of the foot and move. For this reason, a table that can be separated from the middle of the upper platform of the parallel robot and where the foot can be placed was designed.

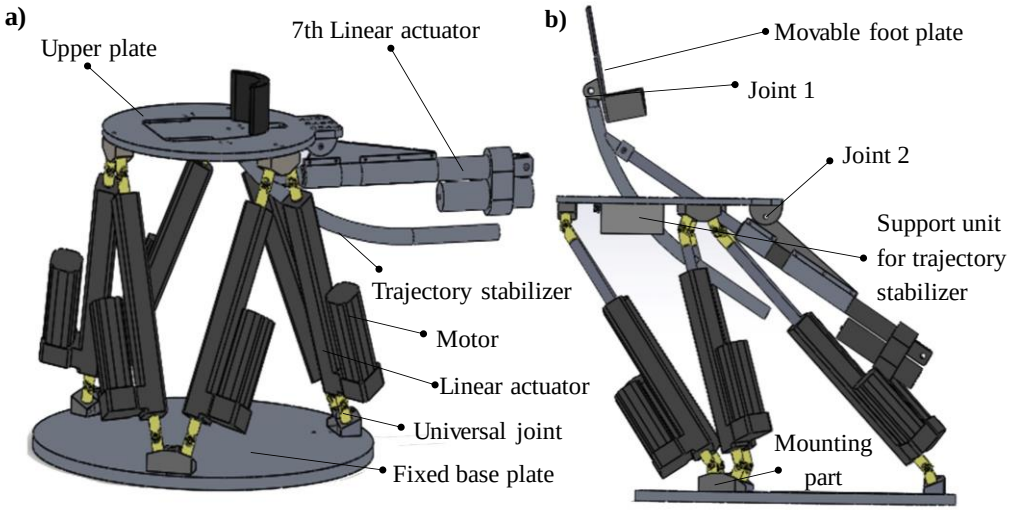

Fig. 2. Mechanical structure of the rehabilitation robot (Budaklı & Yılmaz, 2021).

The footplate is connected to the additional mechanism with a hinge-type joint from the lower part. A split weight through which the additional mechanism in the middle of the upper platform can move. In Fig. 3, balancing weight, teflon bed and reel connected with steel rope from the lower part of the patient chair are shown.

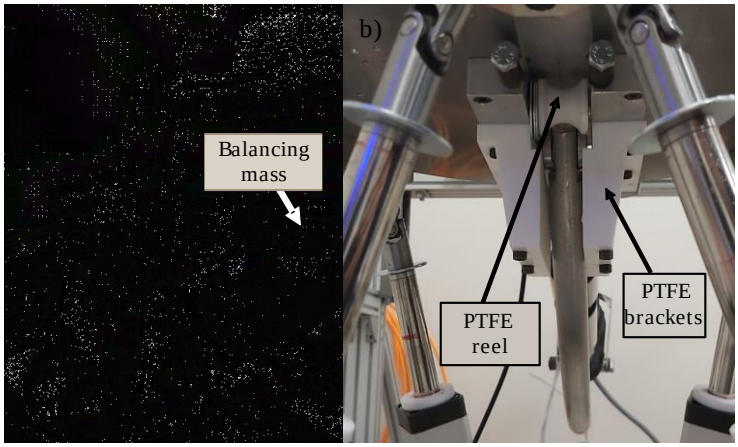

Fig. 3. Rehabilitation robot: a) Balancing weight, b) Teflon bed and reel supporting unit (Budaklı & Yılmaz, 2021).

In addition to the software and electronic safety measures of the rehabilitation robot, some safety measures have also been taken in its mechanical design. The additional mechanism in the knee extension movement is limited to 90°. The parallel robot linear actuator stroke is used as 200 mm, so that the maximum angle in ankle movement does not exceed 40°. There are manual emergency buttons on the right side of the rehabilitated person, on the top of the electronic panel, and also on the user's desktop.

3. MATHEMATICAL MODELING OF THE ROBOT

Inverse Kinematics of the Robot

The inverse kinematics of the rehabilitation robot consists of two parts, the Stewart Platform part and the additional mechanism. In the Stewart Platform part, the determination of the stroke length of each linear actuator for the position and orientation of the midpoint of the upper plate is done by inverse kinematics calculations. In Fig. 4, the vectors for the inverse kinematics calculations on the two legs of the Stewart Platform are shown.

Two separate Cartesian coordinate systems are defined for the fixed based and upper platforms. The vectors between the center of the coordinate system (basic coordinate system) located at the center of the lower platform and the joints at the bottom, and along the legs of the platform are denoted by $\vec{a}$, and $\vec{l}$, respectively. The vector $\vec{p}$ extending from the origin of the base coordinate system to the origin of the upper platform are expressed in the basic coordinate system (Budaklı & Yılmaz, 2021). The vector $\vec{b}$ from the origin of the upper platform to the upper joint of the legs is expressed according to the upper platform coordinate system.

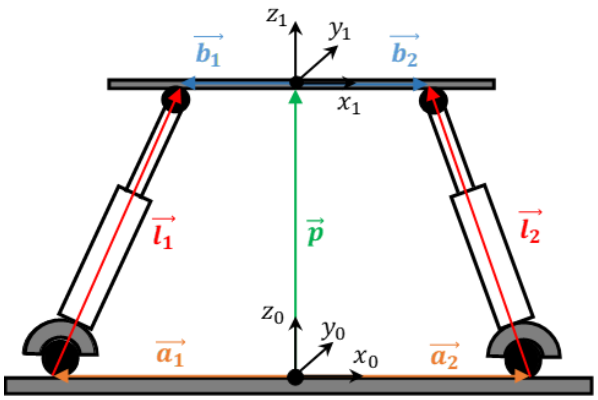

Fig. 4. Vector Definition of Steward Platform for Inverse Kinematics Calculations.

For vector addition, the vector $\vec{b}$ in the upper platform coordinate is defined in the basic coordinate system by multiplying it with the rotation matrix consisting of Euler angles given in (1).

$$\boldsymbol{R} = \begin{bmatrix} \mathrm{c}\,\phi\,\mathrm{c}\,\beta & c\,\phi\,s\,\alpha\,s\,\beta - \mathrm{c}\,\alpha\,\mathrm{s}\,\phi & \mathrm{s}\,\alpha\,\mathrm{s}\,\phi + \mathrm{c}\,\alpha\,\mathrm{c}\,\phi\,\mathrm{s}\,\beta \\ \mathrm{c}\,\beta\,\mathrm{s}\,\phi & \mathrm{c}\,\alpha\,\mathrm{c}\,\phi + \mathrm{s}\,\alpha\,\mathrm{s}\,\phi\,\mathrm{s}\,\beta & \mathrm{c}\,\alpha\,\mathrm{s}\,\phi\,\mathrm{s}\,\beta - \mathrm{c}\,\phi\,\mathrm{s}\,\alpha \\ \mathrm{s}\,\beta & \mathrm{c}\,\beta\,\mathrm{s}\,\alpha & \mathrm{c}\,\alpha\,\mathrm{c}\,\beta \end{bmatrix} \tag{1}$$

The position of each leg of the platform in three axis is achieved with vectorial calculation as,

$$\boldsymbol{L_i} = \mathbf{R} \cdot \vec{\boldsymbol{b}}_{\boldsymbol{i}} + \vec{\mathbf{p}}_{\boldsymbol{i}} - \vec{\mathbf{a}}_{\boldsymbol{i}} \tag{2}$$

$$\begin{bmatrix} L_{ix} \\ L_{iy} \\ L_{iz} \end{bmatrix} = \begin{bmatrix} R_{x1} & R_{y1} & R_{z1} \\ R_{x2} & R_{y2} & R_{z2} \\ R_{x3} & R_{y3} & R_{z3} \end{bmatrix} . \begin{bmatrix} b_{ix} \\ b_{iy} \\ b_{iz} \end{bmatrix} + \begin{bmatrix} p_x \\ p_y \\ p_z \end{bmatrix} - \begin{bmatrix} a_{ix} \\ a_{iy} \\ a_{iz} \end{bmatrix} \tag{3}$$

The leg lengths are as;

$$st_i = \sqrt{{L_{ix}}^2 + {L_{iy}}^2 + {L_{iz}}^2} \quad ,(i = 1,2,..,6) \tag{4}$$

$$st_i = l_i$$

calculated.

In ankle rehabilitation exercises, only the movement of the Stewart Platform is sufficient. Therefore, the inverse kinematics equations above are used. However, knee motion is provided with Stewart and 7th linear actuators. Therefore, additional kinematic equations are required. In the extension movement of the knee joint (see Fig. 5), the Stewart Platform starts to move in the negative *x*-direction at point A and the 7th linear actuator is activated when the foot is at point C after Stewart brings the knee up to $\Theta°$ alone. Through the medium of the 7th actuator and the inclined part in the form of a quarter circle mounted on it, the foot performs the remaining knee orbit after $\Theta°$ in direct proportion to the extension of the piston.

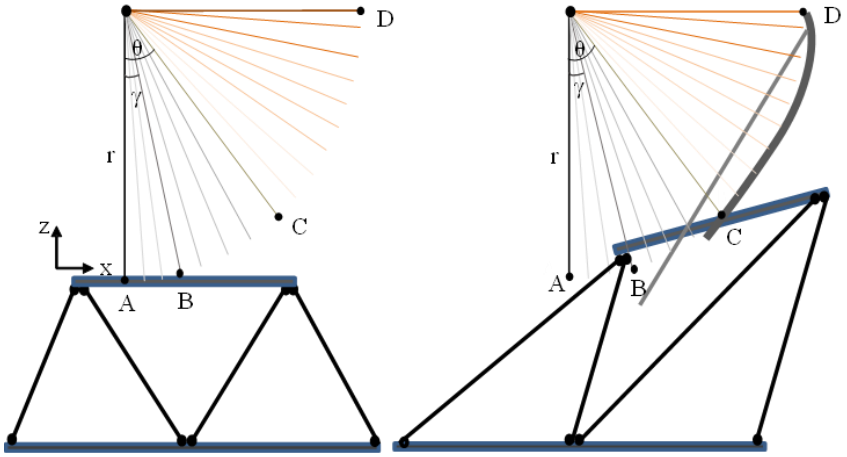

Fig. 5. Trajectory of the Robot for Knee Movement (Budaklı & Yılmaz, 2021).

It reaches the maximum point D. Between the D point and the A point, the 90° angle, which is the maximum value in knee extension movement, is achieved. In Fig. 5, "r" denotes leg length. The deflection values, which vary according to the elongation amount of the piston of the seventh linear actuator, were calculated by polynomial regression and the polynomial is;

$$sp_x = -71{,}26 - 0{,}211S + 0{,}0066S^2 - 0{,}00002015S^3 + 0{,}000000013S^4 \quad (5)$$

Here "S" is the elongation amount of the 7th linear actuator. In order to eliminate the deviations with this obtained polynomial, the 7th linear actuator and the motion of the Stewart platform were obtained as a mathematical expression and placed in the control software of the robot. The displacement of the Stewart Platform in the *x*-axis is as,

$$x_{st} = x_{st43} + sp_x \quad (6)$$

expressed. The amount of elongation of the 7th linear actuator required for the position of the foot, which is accepted as the end processor, depending on the change in knee angle is by

$$S = (\theta - 43) \cdot \frac{24}{43} + 6 \quad (7)$$

calculated. The elongation amount of each linear actuator is obtained by using the vectorial calculation (2) and (7).

Forward Kinematics of the Robot

Different mathematical methods are used to determine the correct leg positions in the forward kinematic calculations of the Stewart parallel robot. The forward kinematics equation can be calculated numerically with an accuracy of 10^{-4} using the Newton-Raphson method (Sarhan & Alwan, 2019). Since this sensitivity is suitable for the rehabilitation robotic system, the Newton-Raphson method was used for advanced kinematic calculations in this study. According to this method, firstly inverse kinematics calculations are set to zero, and defined as

$$f(x)_i = 0 \quad (8)$$

$$\begin{aligned} f(x)_i = [&(p_x + R_{x1} \cdot b_{ix} + R_{y1} \cdot b_{iy} + R_{z1} \cdot b_{iz} - a_{xi})^2 \\ &+ (p_y + R_{x2} \cdot b_{ix} + R_{y2} \cdot b_{iy} + R_{z2} \cdot b_{iz} - a_{iy})^2 \\ &+ (p_z + R_{x3} \cdot b_{ix} + R_{y3} \cdot b_{iy} + R_{z3} \cdot b_{iz} - a_{iz})^2]^{0.5} - l_s - q_i \end{aligned} \quad (9)$$

a function. The function *f*(*x*) is differentiated and its inverse is calculated. The result obtained by dividing f(x) by the derivative of the function *f*(*x*) is obtained from the current upper platform position adn so, it converges to the position of the upper platform. With iteration, the current position of the upper platform is calculated (Alwan & Sarhan, 2019). The position of the midpoint of the Stewart Platform calculated with Newton-Raphson also gives the position of the foot. While it is used directly in this way in ankle rehabilitation exercises, for knee exercises should be determined the knee angle θ. When the 7th linear actuator is in the "0" position, only the Stewart Platform is moving forward kinematics due to knee angle,

$$\theta = \arcsin\left(\frac{x_{st} - x_0}{r}\right) \quad (10)$$

and due to the elongation of the 7th actuator is calculated via

$$\theta = (s-6)\cdot\frac{43}{24}+47\ . \tag{11}$$

4. CONTROL TECHNIQUE

In active rehabilitation exercises, the individual actively moves the limb by using the musculoskeletal system.

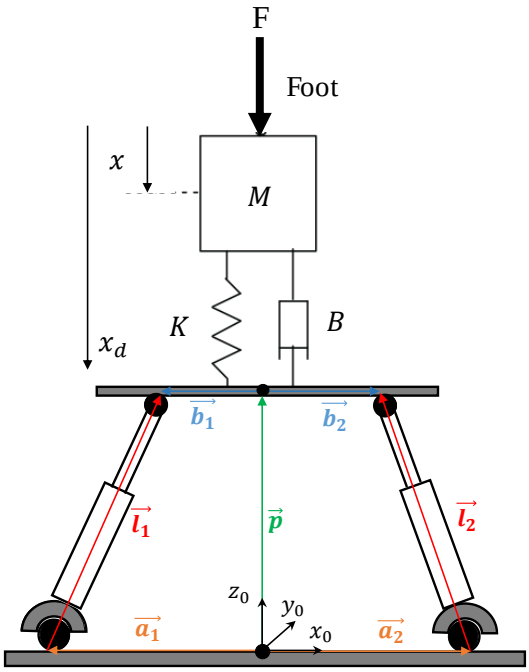

Fig. 6. Mass-Damping-Spring System Between Parallel Robot and Foot.

The rehabilitation robot can act passively in such exercises, as well as apply a certain counterforce. Impedance control structure is designed for the rehabilitation robot to perform active rehabilitation movements. As shown in Fig. 6, a second-order mass-damping-spring system is placed between the environment and the robot in impedance control (Song et al., 2017). Thus, the robot provides movement depending on the force by absorbing the effect of the external *F* force, and the resistance of the robot can be adjusted with the desired coefficients (Ba et al., 2018; Yoshikawa, 2000). Second-order mass-damper-spring equation is as,

$$M(\ddot{x_d}-\ddot{x})+B(\dot{x_d}-\dot{x})+K(x_d-x)=F \tag{12}$$

defined and in the frequency domain,

$$Z(s)=\frac{X(s)}{F(s)}=\frac{1}{Ms^2+Bs+K} \tag{13}$$

defined as an impedance filter. The impedance filter $Z(s)$ updates the position of the robot specified by (12). The mechanical impedance determined by *M*, *B*, and *K* defines how the robot will respond to external forces acting on contact with an object (Kizir & Bingül, 2014). The natural frequency and damping ratio of the second-order system are, respectively,

$$\omega_n=\sqrt{\frac{K}{M}}\ ,\xi=\frac{B}{2B\omega_n} \tag{14}$$

given in the form. Stability conditions of position-based impedance control is as,

$$\xi \geq 0{,}5(\sqrt{1+2k}-1 \tag{15}$$

$$k = K_e/K \gg 1 \tag{16}$$

determined. A position-based impedance control scheme consists of an inner position loop and an outer position based force loop as shown in Fig. 7. The force due to the weight of the foot is accepted as the initial force and considered zero. In this case the desired trajectory X_d is identical to the compliant trajectory X_p since no compliant motions are required. However, in forced motions, a non-zero contact force modifies the desired trajectory in the outer impedance control loop, resulting in the compliant desired trajectory to be tracked by the inner motion control loop according to (12). The applied force is detected in 6 axis by the 6-axis force/torque sensor. Thus, on the axis where the force is applied, the position is adjusted according to the force change.

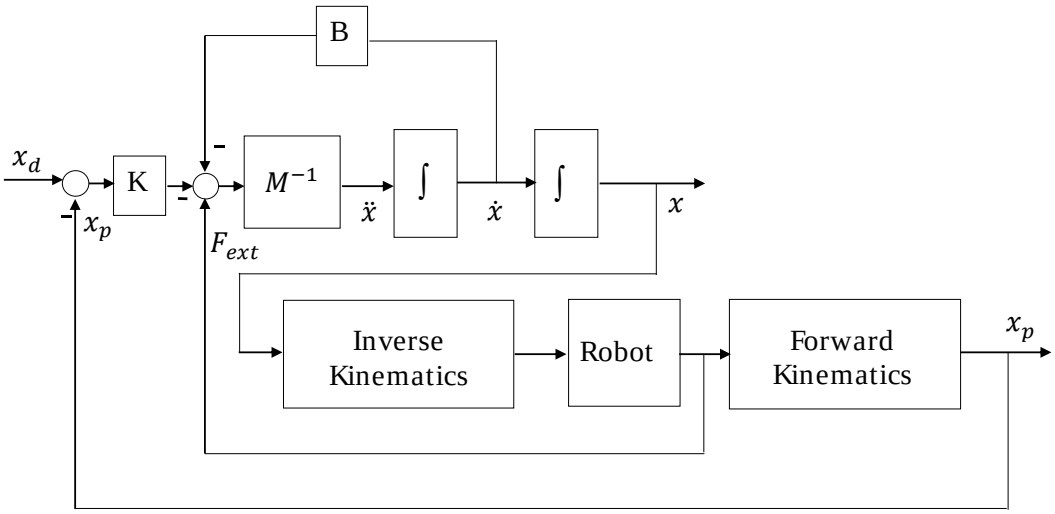

Fig. 7. Block Diagram of Position Based Impedance Control of Parallel Robot.

Position is used as the input value of the system. The position of the midpoint of the platform is subtracted from the desired position and the integration of this difference is taken to form (12). The force of the end point of the platform is measured by the 6-axis force/torque sensor and is included in the equation. Thus, the movement step of the platform is determined and the leg lengths required for this movement are calculated with inverse kinematics and the position-based impedance control is performed by bringing the platform to the desired position with the movement of the linear actuators.

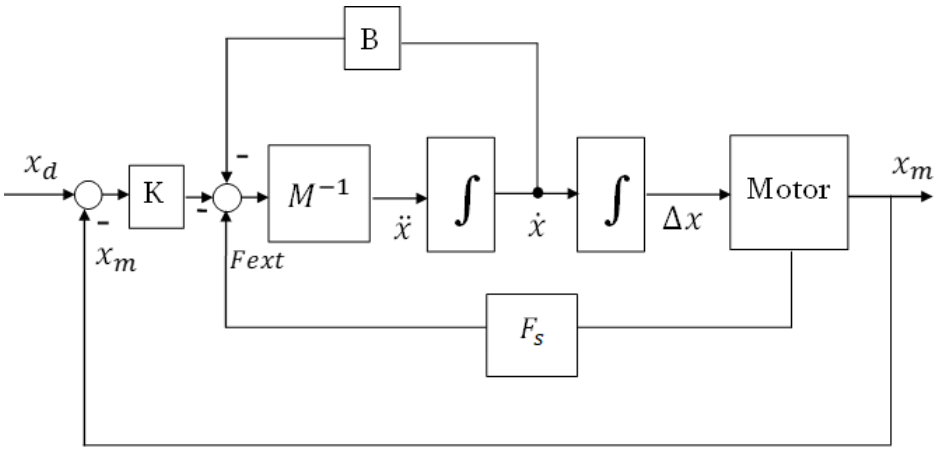

Fig. 8. Block Diagram of Position Based Impedance Control of 7th Linear Actuator.

Fig. 8 shows the position-based impedance control scheme for the 7th linear actuator. According to (12), the mass-damper-spring equation is also valid here. The impedance control structure is created with the force feedback and position feedback received from the end point of the linear actuator. Matlab/Simulink program is used for real-time control of the robotic system. The communication of the force/torque sensor and AC motor drives via Speedgoat takes place via EtherCAT PDO blocks. For real-time control of the robotic system, it is necessary to build a communication topology for the motor drivers so that the Matlab program can work with EtherCAT communication.

In order to use the EtherCAT communication method, a communication topology covering all the engines that will use the communication protocol is first initialized with TwinCAT. The topology of 6 motors to communicate serially was created in the TwinCAT program. In addition, the ".xml" file was created by using PDO objects that transmit the signal at the preferred sampling time for the required control signals. With Matlab/Simulink blocks, necessary input signals are transmitted to motor drivers and output signals are detected. The closed-loop control signals created with these blocks were combined with the necessary Matlab® software to transmit and receive commands to the synchronous motors.

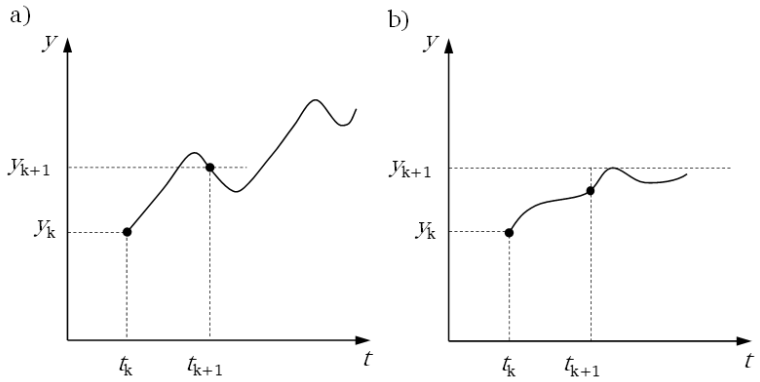

Fig. 9. Synchronization Problem of the Robot Algorithm Software and Simulink Realtime: a) Fast, b) Slow.

However, the Matlab program or the program software created in the user interface does not run with the specified sampling rate for PDOs in Simulink real-time. For this reason, synchronization problem may occur in the detection loop of the motors with the input command. When the software loop rate is faster than the sampling rate of the PDOs, it exceeds the desired position, as in Fig. 9a, causing a less damped motion. When the software loop rate is slower than the sampling rate of the

PDOs, it behaves like an over-damped system and cannot reach the desired position at the sampling rate, as shown in Fig. 9b. In order to solve this problem, the parts of the software program that need to work simultaneously can be placed in the Matlab/Simulink function within the Simulink realtime program and controlled by the software in the user interface. Thus, synchronization is performed and vibration is completely prevented in active rehabilitation exercises.

5. RESULTS AND DISCUSSION

In this experimental study with healthy individuals, the ability of the rehabilitation robot to perform active and active-assisted ankle and knee rehabilitation exercises was evaluated. In active exercises, healthy volunteers experienced bringing the robot to standard ROM of the joint by guiding the robot with the movement of their lower extremities. In the active assisted exercises, the volunteers first guided the robot with their own movements and brought the joint angle to a value lower than the standard ROM of the joint. The robot realized that the movement stopped and that no force or torque was applied in the same direction, and completed the relevant movement within the framework of the required ROMs and performed the active-assisted rehabilitation exercise. In graphics; the first volunteer was expressed as G-1 and the second volunteer as G-2.

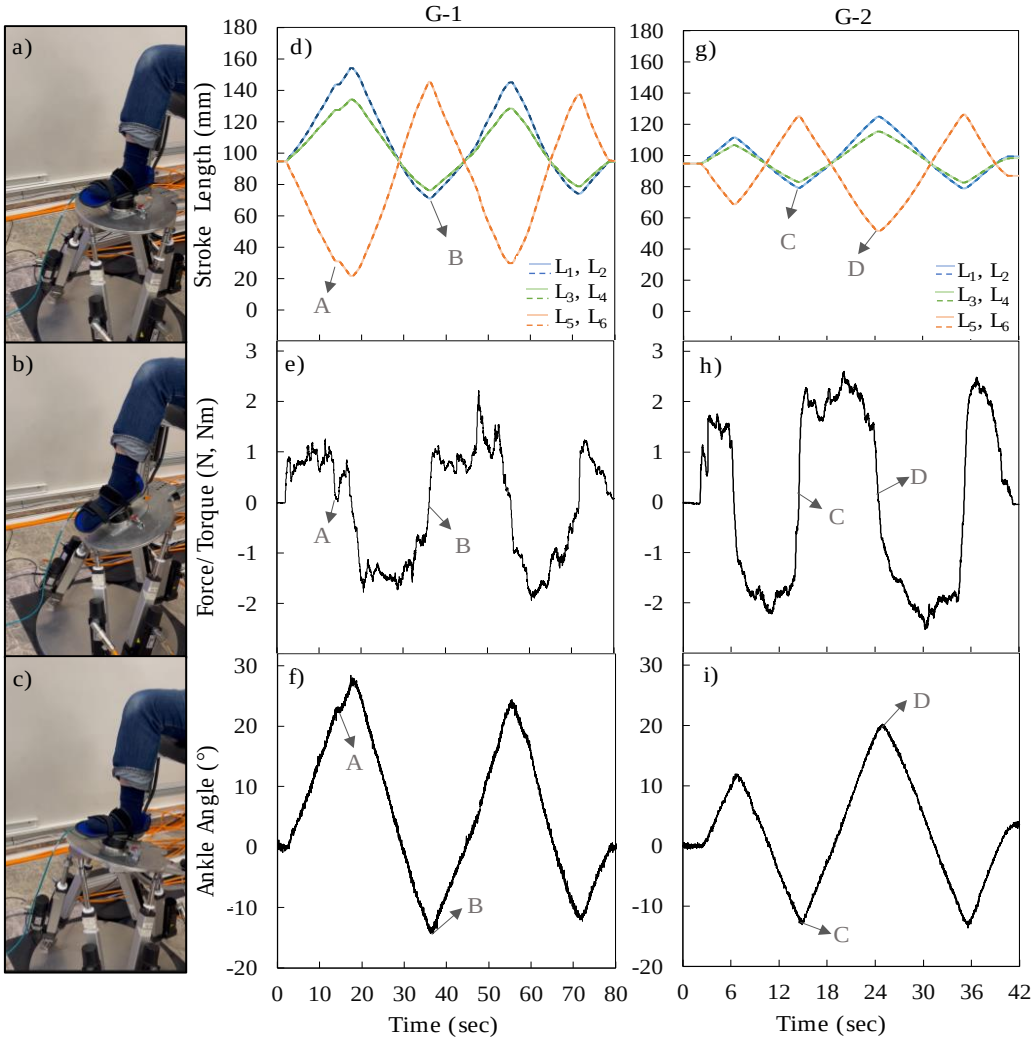

Fig. 10. Plantarflexion-Dorsiflexion Active Exercise, a), b), c) Representative Foot Position of the Patient, d), g) Stroke Lengths, e), h) Force/Torque Sensor, f), i) Ankle Angle.

Fig. 10 shows the results of experiments with two volunteers in active exercise for plantarflexion-dorsiflexion movement of the ankle. Fig. 10d and g show the piston length of linear actuators of the Stewart platform in the first and second volunteer experiments, respectively. Since the motion is rotational motion in the *y*-axis, linear actuator pistons (L1-L2, L3-L4 and L5-L6) symmetrical with respect to the *x*-axis have equal elongation. The first volunteer performed the plantarflexion movement shown in Fig. 10b in the first 18 seconds and the second volunteer in the first 7 seconds. Accordingly, the L1 and L2 pistons at the rear realized the maximum elongation, while the L5 and L6 at the front reached the minimum value.

Fig. 10e and h show the torque exerted by the foot in the T_y direction, it was observed that the first volunteer applied a torque of approximately 1.2 Nm in the positive direction of T_y, and the second volunteer applied a torque of 1.7 Nm. In Fig. 10d-f, at the point indicated by "A", the change in the pistons, force/torque sensor and foot angle was observed when the first volunteer changed the force applied. At the points marked "B", "C" and "D", changes in motion are shown. When the volunteers started to move in the opposite direction, opposite changes in strength and positions were observed. In this motion, torque and force parameters of the 6-axis force/torque sensor, except T_y, are not included in the control algorithm. In this way, while plantarflexion-dorsiflexion movement is performed, unwanted movements of the parallel robot in other axis are prevented. The first volunteer performs the dorsiflexion movement in Fig. 10c between 18 and 37 seconds, and the second volunteer between 7 and 15 seconds. L1 and L2 have minimum elongation, while L5 and L6 pistons show maximum elongation. It was observed that the first and second volunteers exerted an average torque of −1.8 and −2.2 Nm in the negative direction of T_y, respectively. Volunteers repeated the plantarflexion-dorsiflexion movement twice. Fig. 10f and i show that the foot angle varied between 30° and −16° in the first volunteer, and between 24° and −14° in the second volunteer, under the control of the volunteers.

The linear actuator strokes (L1-L2, L3-L4 and L5-L6) symmetrical with respect to the *x*-axis have equal stroke lengths, since the motion is rotational motion in the *y*-axis with respect to the platform axis (see Fig. 11d and g). The first volunteer performed the plantarflexion active exercise between the 9th and 15th seconds and stopped the movement at the "A" point. Between 15 and 19 seconds, the robot switched to assisted mode because the movement did not continue and there was no increase in the force value.

He brought the ankle to the required ROM at the "B" point in the 40th second, after applying 15 seconds of stretching, he brought the ankle to the starting position. Between the 89th and 93rd seconds, the volunteer actively dorsiflexed and stopped the movement at the "C" point. Between the 93rd and 98th seconds, the robot switched to the assisted mode because the movement did not continue and there was no change in the force value, brought the ankle to the required ROM at the 110th second, and brought the ankle to the starting position after 15 seconds of stretching.

The second volunteer performed the plantarflexion active exercise between 1.2 and 7 seconds and stopped the movement at the "D" point. Between the 7th and 10th seconds, the robot switched to assisted mode because the movement did not continue and the force value did not increase. He brought the ankle to the required ROM at the "E" point at 35 seconds, after applying 15 seconds of stretching, he brought the ankle to the starting position. Between the 82nd and 87th seconds, the volunteer actively dorsiflexed. At the “F” point, there was a change in the force in the opposite direction and this movement caused vibration. Between the 87th and 91st seconds, the robot switched to the assisted mode because the movement did not continue and there was no change in the force value, brought the ankle to the required ROM at the 103rd second, and brought the ankle to the starting position after 15 seconds of stretching. The force/torque sensor data during this time is

in Fig. 11e and h. In the graphs, the changes in the force/torque sensor of the volunteers during active exercise are shown at the "A", "C", "D", "F" points. Fig. 11f and i show the changes in foot angle during the exercise. After the first volunteer actively plantarflexed up to 7°, it was observed that the robot completed the foot angle up to 40° in the plantarflexion movement in Fig. 11a. In the dorsiflexion movement shown in Fig. 11c, after the volunteer actively moved his foot up to −6°, the robot provided ankle motion up to −20°. After the second volunteer made 10° active plantarflexion, it was observed that the robot completed the foot angle up to 40° in the plantarflexion movement in Fig. 11a.

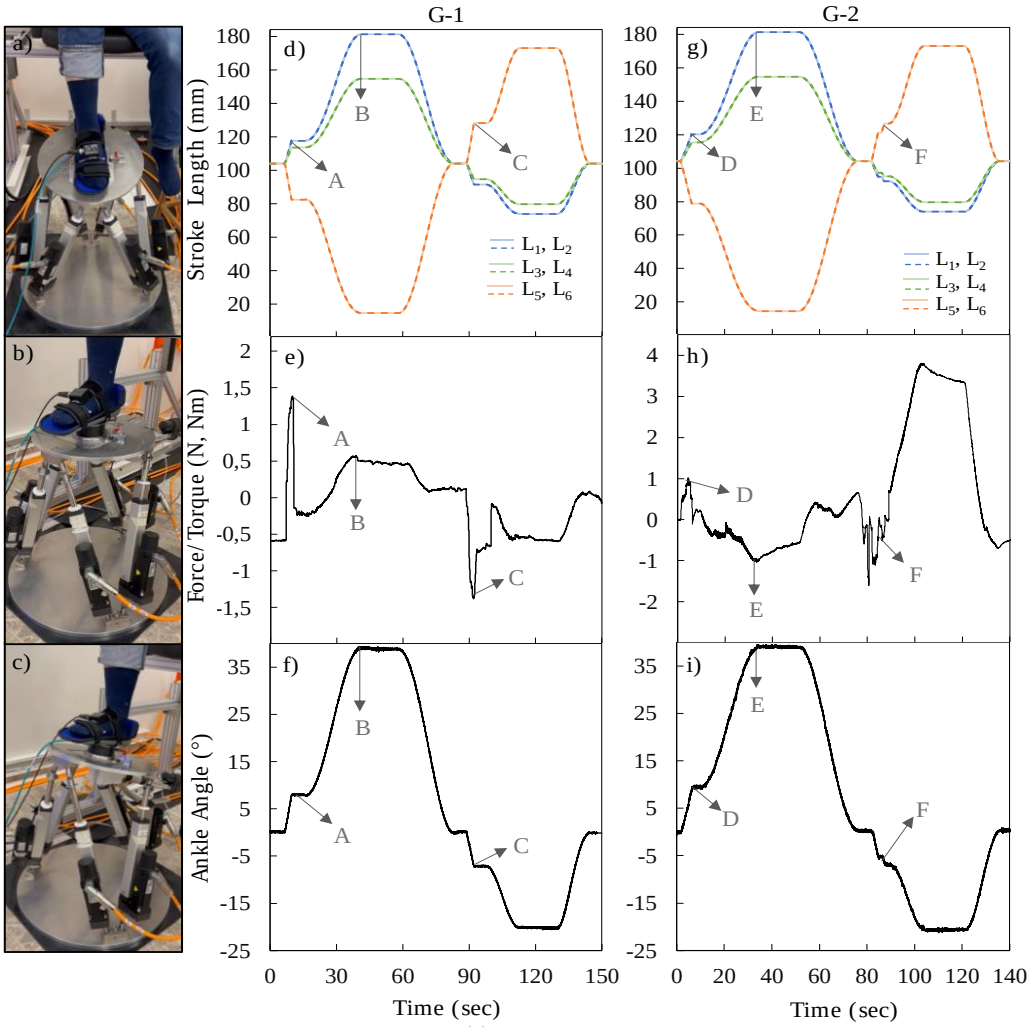

Fig. 11. Plantarflexion-dorsiflexion active-assisted exercise, a), b), c) representative foot position of the patient, d), g) stroke lengths, e), h) force/torque sensor, f), i) ankle angle.

The Fig. 12 shows the graphs obtained when the volunteers performed the eversion-inversion active rehabilitation exercise. The force in the T_x axis is considered. The pistons of the linear actuators do not intersect on the *y*-axis of the coordinate system of the midpoint of the foot on the upper platform, so the piston lengths did not change symmetrically (see Fig. 12d and g). While L1 and L3 reached the maximum value in inversion movement, L2 and L4 showed minimum elongation. The first volunteer performs the inversion movement in Fig. 12a in the first 20 seconds and the second volunteer in the first 7 seconds. The point at which the maximum angle is reached in this movement is indicated by "A" for the first volunteer and "C" for the second volunteer.

It was observed that the volunteers applied torque of approximately ±1.5 Nm in the positive and negative direction of T_x. Angular changes in the ankles of the volunteers are given in the graphs in Fig. 12f and i, respectively. Accordingly, the angular change in the ankle of the first volunteer ranged from a maximum of +30° to −15°, and the maximum range of +15° to −16° in the second volunteer. In this movement, the axis of the 6-axis force/torque sensor other than the *x*-axis are not included in the control algorithm. In this way, while the eversion-inversion movement is performed, the forces of the other axis of the parallel robot are detected and unwanted movements are prevented. Volunteers repeated the eversion-inversion movement twice and ended it by returning to the starting position.

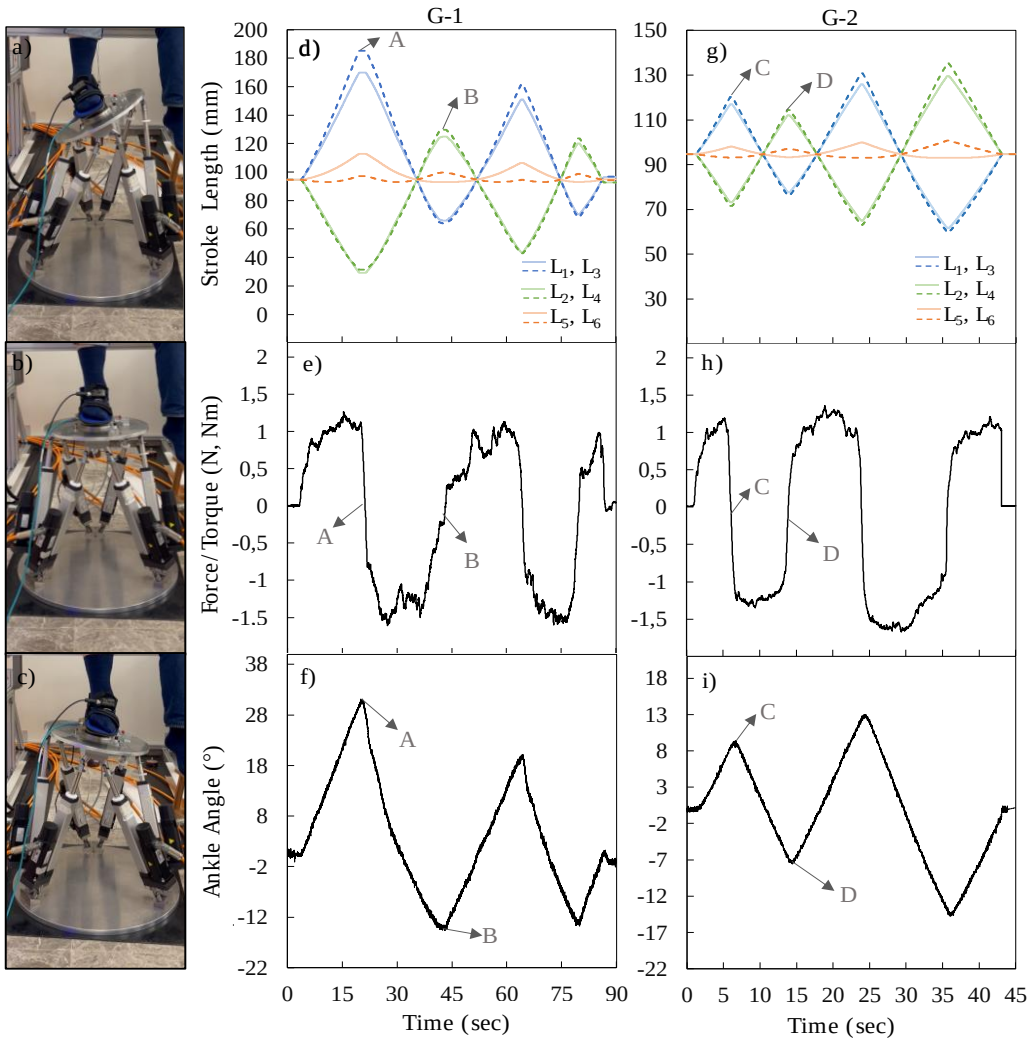

Fig. 12. Eversion-inversion active exercise, a), b), c) representative foot position of the patient, d), g) stroke lengths, e), h) force/torque sensor, f), i) ankle angle.

Fig. 13 shows the results of active-assisted rehabilitation exercise for eversion-inversion movement of the ankle. The first volunteer performed the voluntary inversion active exercise between 8 and 16 seconds and stopped the movement at the "A" point. Between 16 and 20 seconds, the robot switched to assisted mode because the movement did not continue and there was no increase in the force value. He brought the ankle to the required ROM at the "B" point at 38 seconds, after applying 15 seconds of stretching, he brought the ankle to the starting position.

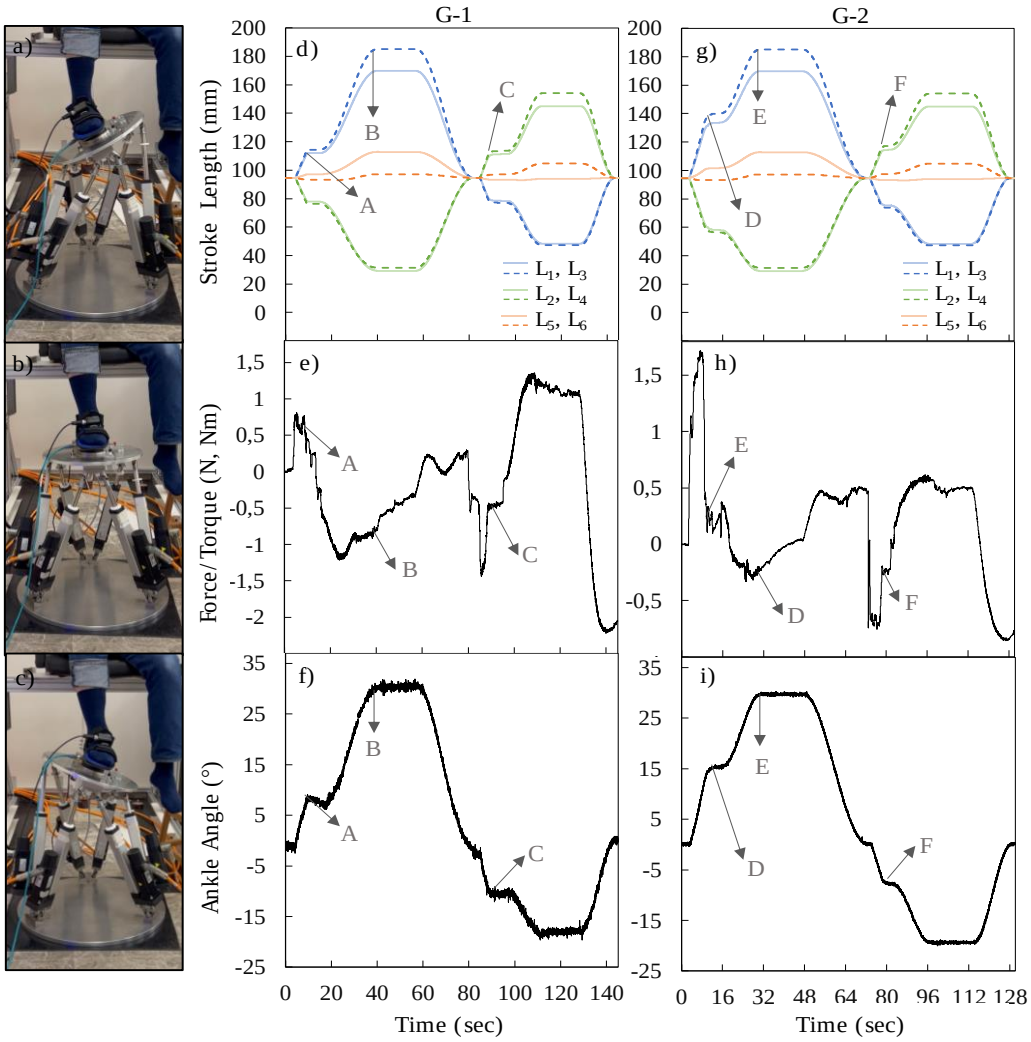

Fig. 13. Eversion-inversion active-assisted exercise, a), b), c) representative foot position of the patient, d), g) stroke lengths, e), h) force/torque sensor, f), i) ankle angle.

Between the 82nd and 89th seconds, the volunteer actively dorsiflexed and stopped the movement at the "C" point. Between the 89th and 93rd seconds, the robot switched to the assisted mode due to the lack of movement and no increase in the strength value, brought the ankle to the required ROM at the 112th second, and brought the ankle to the starting position after 15 seconds of stretching. The second volunteer performed the plantarflexion active exercise between 2.5 and 11 seconds and stopped the movement at the "D" point. Between the 11th and 15th seconds, the robot switched to assisted mode because the movement did not continue and there was no increase in the force value. He brought the ankle to the required ROM at the "E" point in the 31st second, after applying 15 seconds of stretching, he brought the ankle to the starting position. Between the 74th and 79th seconds, the volunteer actively dorsiflexed to the "F" point. Between the 79th and 82nd seconds, the

robot switched to the assisted mode because the movement did not continue and there was no increase in the strength value, brought the ankle to the required ROM at the 97th second, and brought the ankle to the starting position after 15 seconds of stretching. The force/torque sensor data during this time is in Fig. 13e and h. In the graphs, the changes in the force/torque sensor of the volunteers during active exercise are shown at the "A", "C", "D", "F" points.

Fig. 13f and i show the changes in foot angle during exercise. It was observed that the first volunteer completed the robot's foot angle up to 30° after actively performing the inversion movement in Fig. 13a up to 8,5°. In the eversion movement shown in Fig. 13c, after the volunteer actively moved his foot up to −11°, the robot provided ankle motion up to −20°. It was observed that the second volunteer completed the foot angle of the robot up to 30° after 16° of active inversion movement. In the eversion movement shown in Fig. 13c, after the volunteer actively moved his foot up to −7.5°, the robot provided ankle motion up to −20°. Adduction-abduction active exercises for ankle are given in Fig. 14. Relevant movements are realized by rotation of the foot in positive and negative directions relative to the *z*-axis of the coordinate system located at the midpoint of the parallel platform. The first volunteer performed the adduction movement in the first 10 seconds and the second volunteer in the first 8 seconds. It has been shown that just before the "A" point in the graphics, the torque applied by the foot of the first volunteer decreased and accordingly the linear change in the angle of the piston and the foot deteriorated, and the movement continued with the application of a positive torque at the "A" point again.

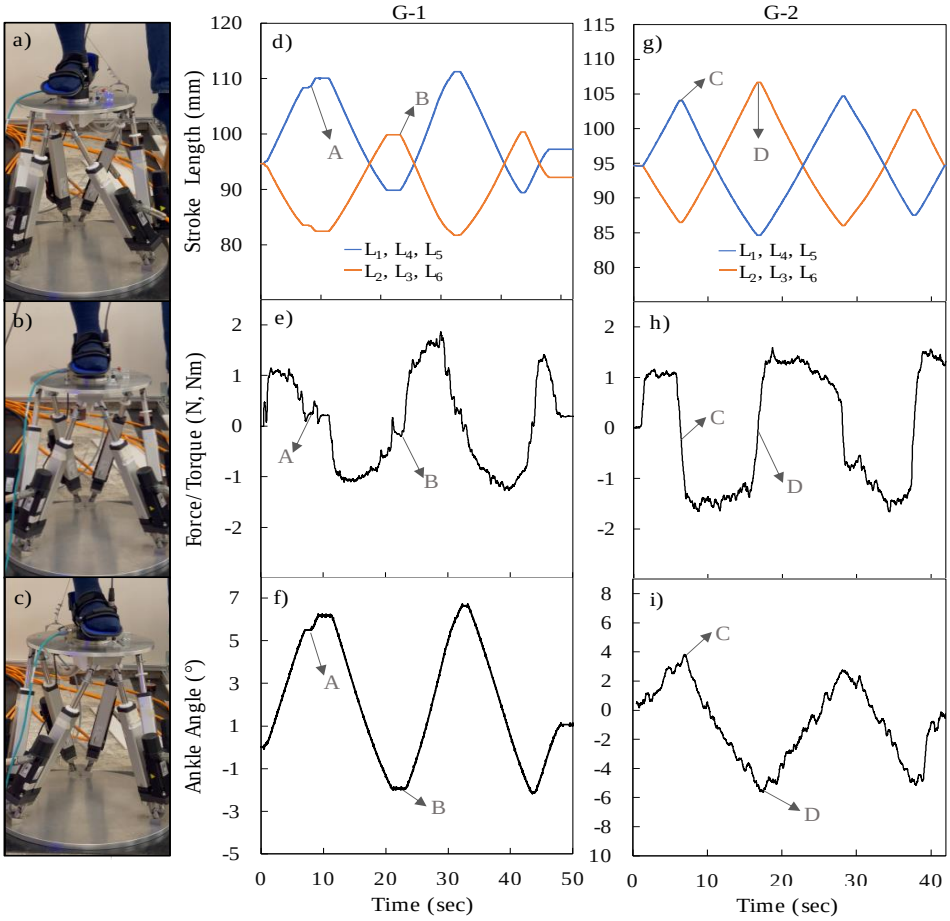

Fig. 14. Abduction-adduction active exercise, a), b), c) representative foot position of the patient, d), g) stroke lengths, e), h) force/torque sensor, f), i) ankle angle.

The first volunteer performed the abduction movement between 17 and 20 seconds, and the second volunteer between 11 and 17 seconds, and repeated the adduction-abduction movement serially. Fig. 14e and h show the torque exerted by the volunteers on the *z*-axis. It was observed that the foot of the first volunteer exerted a maximum torque of 2 Nm to −1.2 Nm, and the second volunteer applied a maximum torque of 1.8 Nm to −1.7 Nm. The changes in foot angles are shown in Fig. 14f and i. Accordingly, the angular position of the foot of the first volunteer varied between 7° and −3°, while the angular position of the second volunteer changed between 4° and −5.7°. The graphs in Fig. 14 show the reverse movement of the pistons and foot angles while changing the directions of the torques applied by the first and second volunteers at the "B", "C" and "D" points. Fig. 15 shows the results of adduction-abduction active-assisted rehabilitation exercise for ankle. The first volunteer performed voluntary adduction active exercise between 3 and 8 seconds and stopped the movement at point "A". Between 8 and 11 seconds, the robot switched to assisted mode because the movement did not continue and there was no increase in the force value. He brought the ankle to the required ROM at the "B" point in the 20^{th} second, after applying the stretch for 15 seconds, he brought the ankle to the starting position. Between the 51^{st} and 54^{th} seconds, the volunteer actively performed the abduction movement and stopped the movement at the "C" point. Between the 54^{th} and 62^{nd} seconds, the robot switched to the assisted mode due to the lack of movement and no increase in the strength value, brought the ankle to the required ROM at the 73^{th} second and brought the ankle to the starting position after 15 seconds of stretching. Second volunteer, 1.8 to 7.5. performed the adduction active exercise between seconds and stopped the movement at the "D" point.

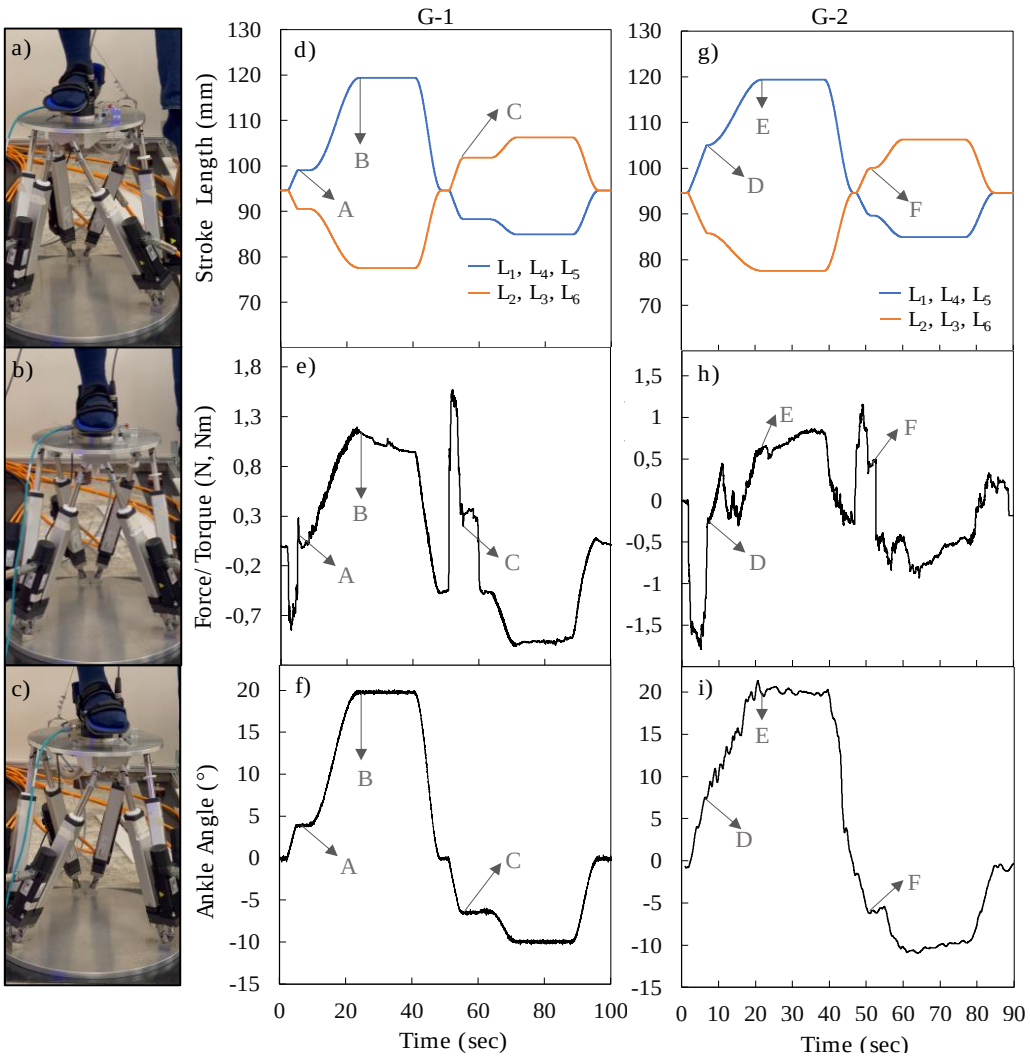

Fig. 15. Abduction-adduction active-assisted exercise, a), b), c) representative foot position of the patient, d), g) stroke lengths, e), h) force/torque sensor, f), i) ankle angle.

Between 7.5 and 9 seconds, the robot switched to assisted mode because the movement did not continue and there was no increase in the force value. He brought the ankle to the required ROM at the "E" point at 22 seconds, after applying 15 seconds of stretching, he brought the ankle to the starting position. 47 and 51.5. Between seconds, the volunteer actively performed the abduction movement up to the "F" point. Between 51.5 and 53 seconds, the robot switched to assisted mode because the movement did not continue and there was no increase in the strength value, brought the ankle to the required ROM at 60 seconds, and brought the ankle to the starting position after 15 seconds of stretching. The force/torque sensor data during this time is in Fig. 15e and h. In the graphs, the changes in the force/torque sensor of the volunteers during active exercise are shown at the "A", "C", "D", "F" points. Fig. 15f and i show the changes in foot angle during exercise. It was observed that the first volunteer completed the foot angle of the robot up to 20° after actively performing the adduction movement up to 4°. After actively moving the volunteer foot up to −6.5° in abduction movement, the robot provided ankle motion up to −10°. It was observed that the second volunteer completed the foot angle of the robot up to 20° after 7° of active adduction movement. In the abduction movement, after the volunteer actively moved his foot up to −6°, the robot provided ankle motion up to −10°. The pistons L1-L2, L3-L4 and L5-L6 showed the same

elongation as the upper platform was symmetrical in the x-axis during movement (see Fig. 16d and g). Figure 5.7e and h show the force/torque variations in the three axis of the 6-axis force/torque sensor position-based impedance control for two volunteers. While performing the knee extension joint movement, the volunteers performed the movement by making linear motion in the *y*-axis (*x*-axis of the platform) and *z*-axis and rotation in the *x*-axis (*y*-axis of the platform) of the force/torque sensor.

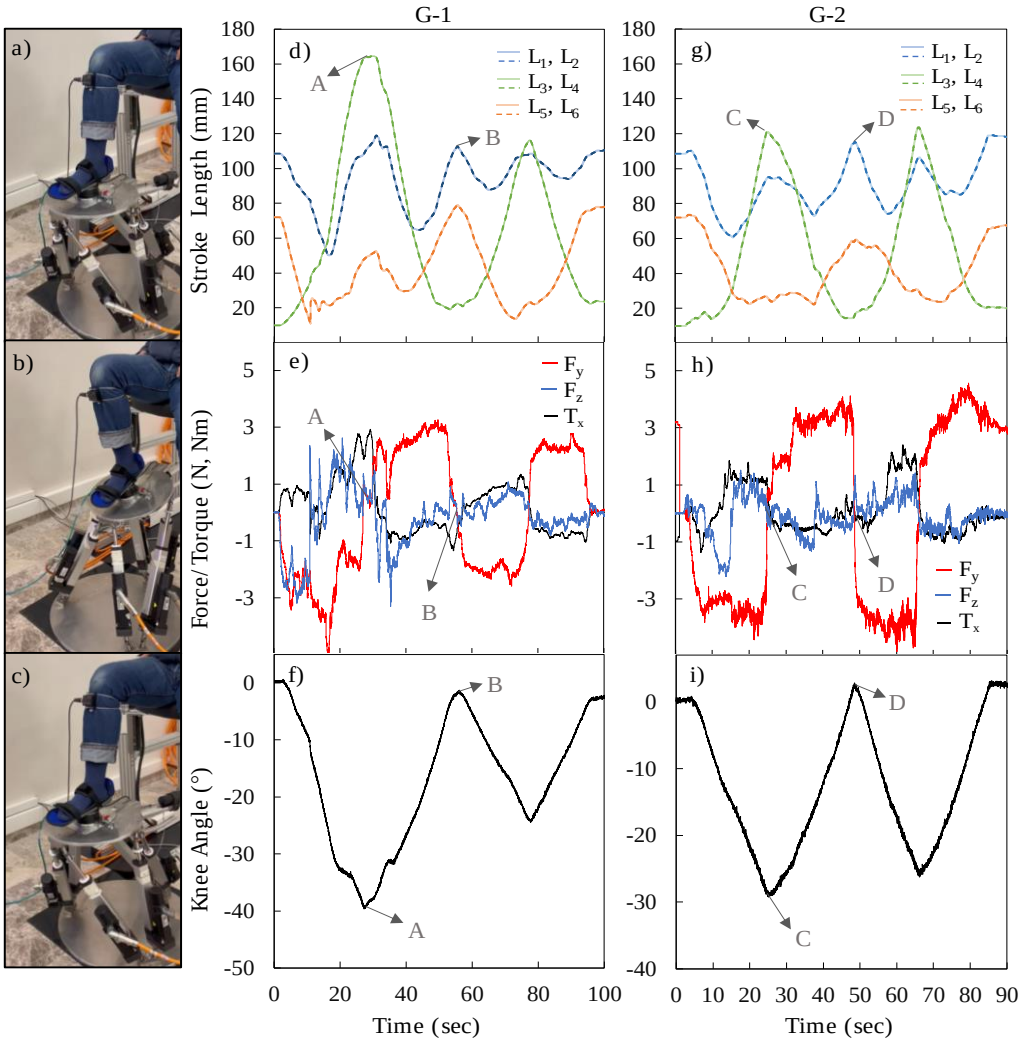

Fig. 16. Knee flexion active exercise, a), b), c) representative foot position of the patient, d), g) stroke lengths, e), h) force/torque sensor, f), i) Knee angle.

In the graphs, the change in forces and torques in the opposite direction at the points "A", "B", "C" and "D" and the change in the knee angle in Fig. 16f and i in the opposite direction were observed. The most force change occurred in the *y*-axis of the force/torque sensor, with a maximum range of +3.4 N to −4 N for the first volunteer, and +3.7 N to −4 N for the second volunteer. Variations in knee angle for two volunteers are given in Fig. 4.7f and i. In the first 28 seconds, the first volunteer brought his knee to −40° and came to the starting position. He performed the repetition of the movement between 58 and 95 seconds and brought the knee to −25° to the starting position. The second volunteer brought it to −30° in 24 seconds and passed 0° at the "D" point. He started the repetition from this position and performed between 52 and 64 seconds and brought the knee to −25° to the starting position.

Fig. 17 shows the results of active-assisted rehabilitation exercise for flexion movement in the knee joint. The first volunteer performed the knee flexion active exercise between 17 and 30 seconds and stopped the movement at the "A" point at the knee angle of −20°. Between the 30th and 41st seconds, the robot waited for a long time due to the lack of increase in the force value but the change in the angle sensor and switched to the assisted mode. The array brought it to −45° ROM at point "B" at 52 seconds, while the piston lengths remained constant while applying tension. After stretching, he brought the knee back to the starting position at point "C" at 108 seconds and stopped the movement. The second volunteer performed the knee flexion active exercise between 4 and 16 seconds and stopped the movement at the "D" point at −15°. Between 18.5 and 26 seconds, the robot switched to assisted mode because the movement did not continue and the force value decreased. The array brought it to −45° EHA at point "E" at 62 seconds, while the piston lengths remained constant while applying tension.

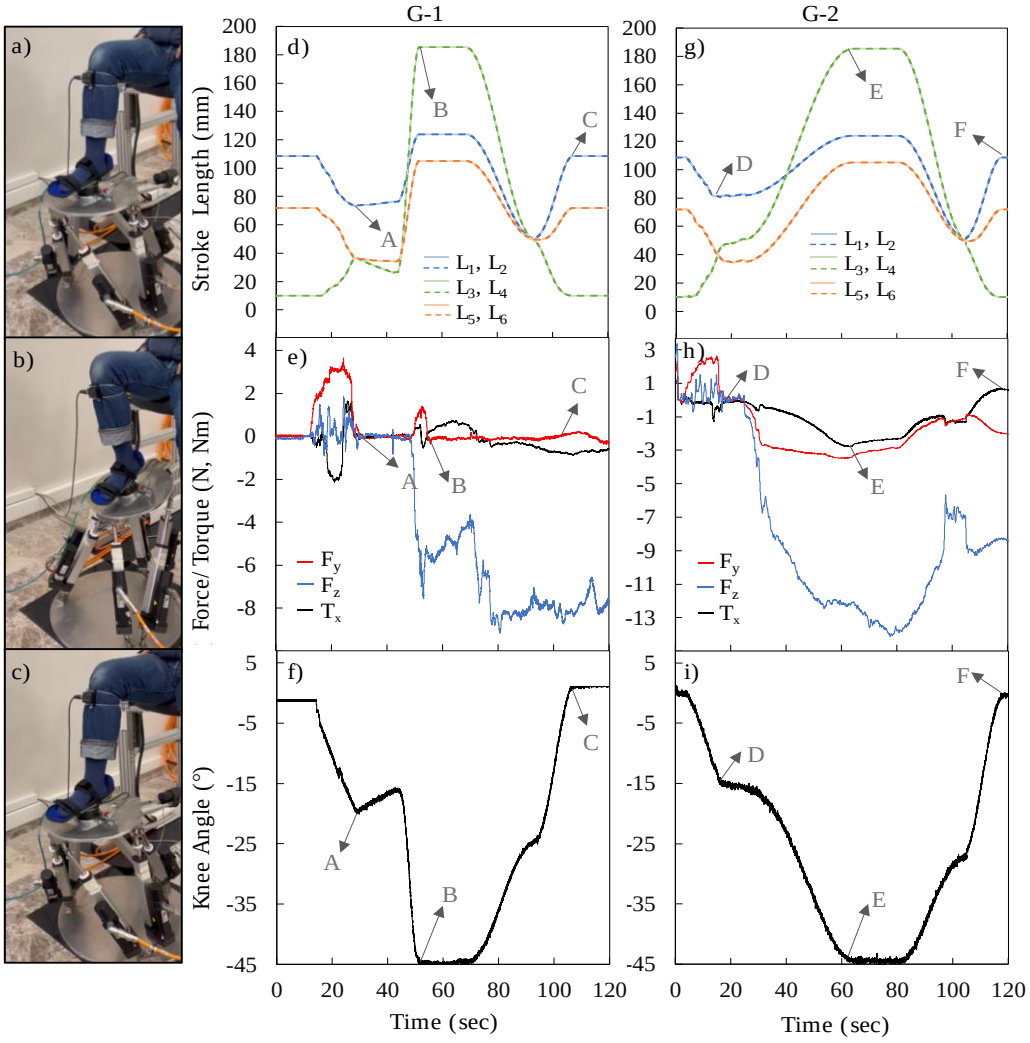

Fig. 17. Knee flexion active-assisted exercise, a), b), c) representative foot position of the patient, d), g) stroke lengths, e), h) force/torque sensor, f), i) Knee angle.

After stretching, he brought the knee back to the starting position at the "F" point at 118 seconds and stopped the movement. Force/torque sensor data for the two volunteers during this time are shown in Fig. 17e and h, respectively. In this motion, linear force sensing in the *y*- and *z*-axis of the 6-axis force/torque sensor and torque sensing in the *x*-axis are used for position-based impedance

control of the parallel robot. At points "A" and "D" in the graphs, the changes in the force/torque sensor are shown while the volunteers are actively exercising. After the first volunteer made the extension movement actively until the "A" point, the robot continued its movement as the force values in the *y*- and *z*-axis approached zero at this point. According to the force/torque sensor axis during the first voluntary active movement; It exerted a maximum force/torque of 3.8 N on the *y*-axis, 2 N on the *z*-axis and −2 Nm on the *x*-axis. After the second volunteer executed the knee flexion movement actively until the "D" point, the robot continued the movement as the force values in the *y*- and *z*-axis approached zero at this point. According to the force/torque sensor axis during the first voluntary active movement; It exerted a maximum force/torque Experimental results of knee extension active exercise are given in Fig. 18. When it starts to move from the starting position, the parallel robot moves first, and when it reaches the "A" point in the first volunteer and "C" in the second volunteer, the seventh linear actuator is activated and the knee extension joint movement is completed. of 2.9 N in the *y*-axis, 1.5 N in the *z*-axis and −1.2 Nm in the *x*-axis. Fig. 4.9e and h show the force/torque variations in the three axis of the 6-axis force/torque sensor position-based impedance control for two volunteers. While performing the knee extension joint movement, the volunteers performed the movement by making linear motion in the *y*-axis (*x*-axis of the platform) and *z*-axis and rotation in the *x*-axis (*y*-axis of the platform) of the force/torque sensor.

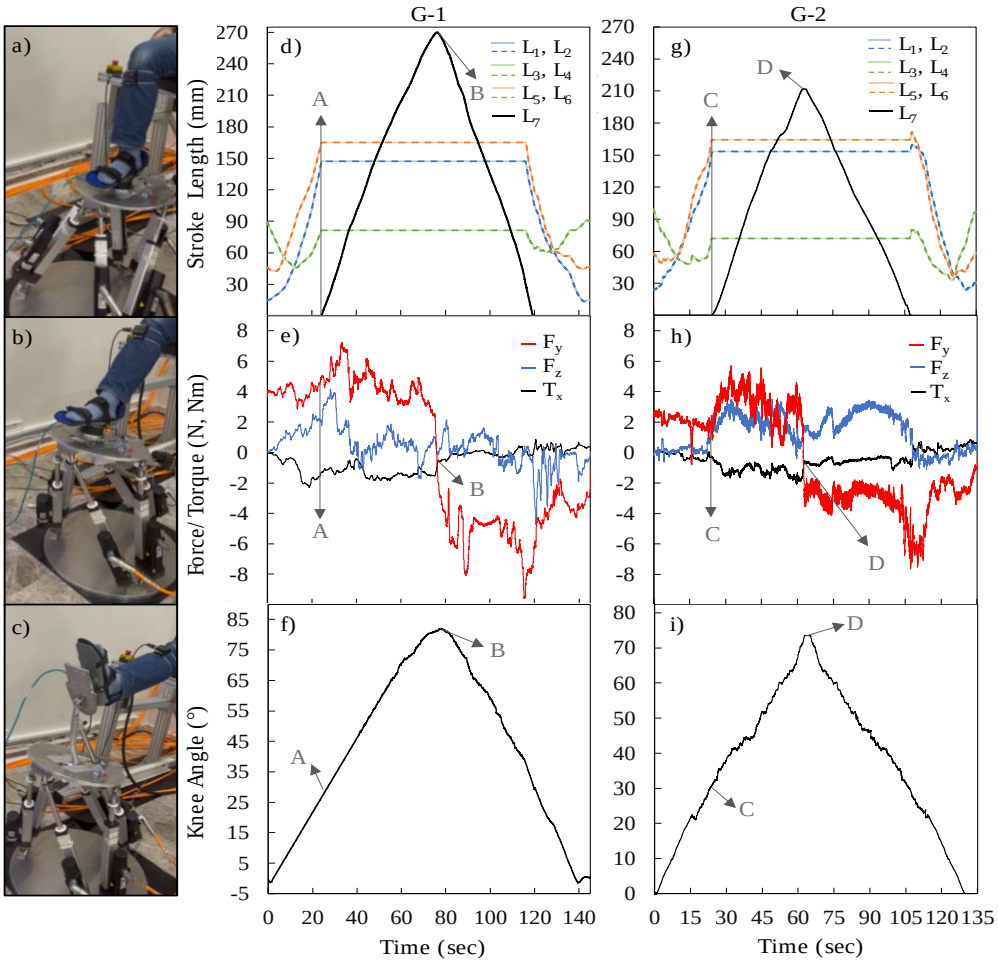

Fig. 18. Knee-extension active exercise, a), b), c) representative foot position of the patient, d), g) stroke lengths, e), h) force/torque sensor, f), i) Knee angle.

With the activation of the seventh linear actuator at points "A" and "C" in the graphics, the change in forces and torques continued in the same way. The change in the *x*- and *y*-axis direction of the force/torque sensor at the "B" and "D" points in the graphs and the movement direction of the seventh linear actuator and the change in the knee angle in Fig. 18f and i in the opposite direction are observed. By providing position-based impedance control with the force and torque values of the relevant axis, the position in the axis is changed according to the forces and torques applied by the person on these axis.

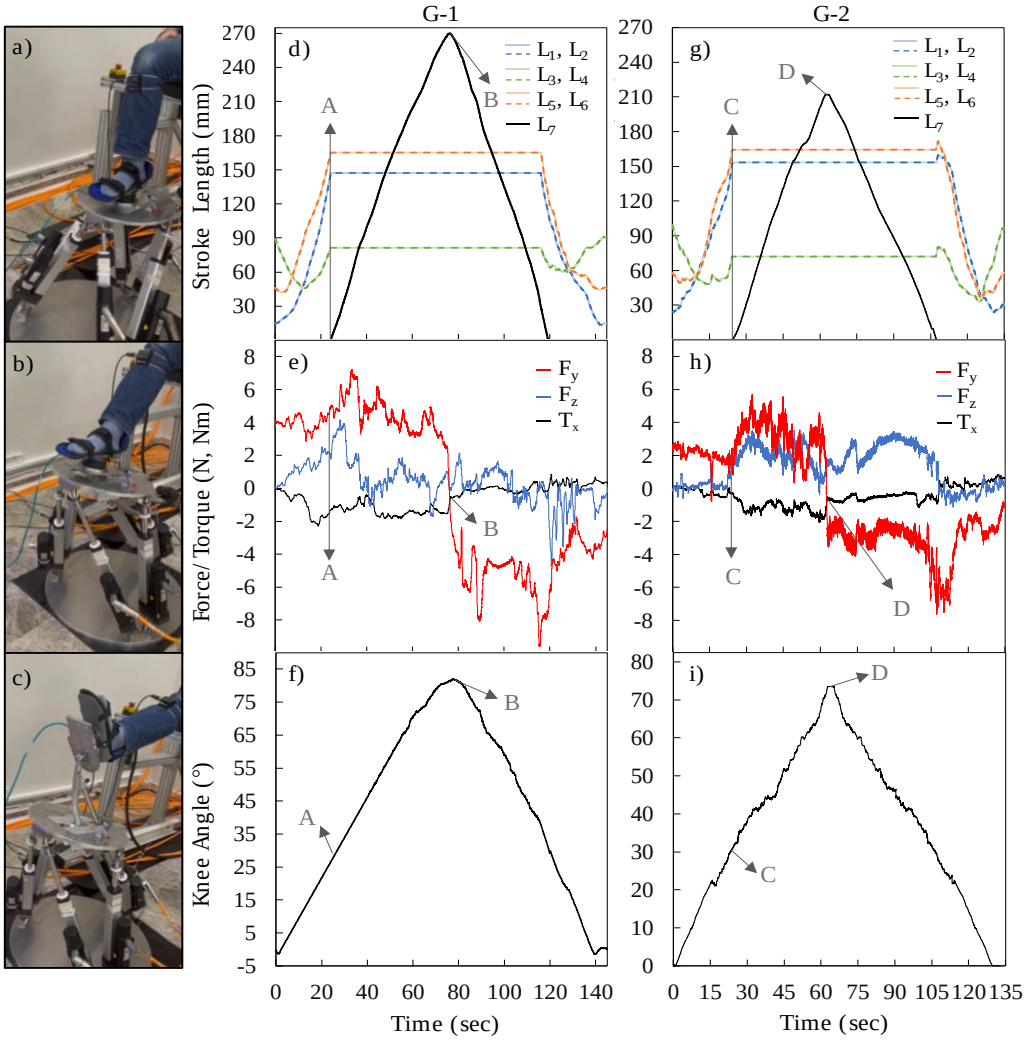

Fig. 19. Knee-extension active-assisted exercise, a), b), c) representative foot position of the patient, d), g) stroke lengths, e), h) force/torque sensor, f), i) Knee angle.

In Fig. 19d and g, the changes in the piston lengths of the robot's linear actuators for the first and second volunteers and the corresponding change in the knee angle are shown in Fig. 4.10f and i. The first volunteer performed the active knee extension exercise between 2 and 38 seconds and stopped the movement at the "A" point at the knee angle of 44°. Between the 38th and 42nd seconds, the robot switched to assisted mode because the movement did not continue and the force value did not increase. The array brought it to 88.7° ROM at point "B" at 56 seconds, while the piston lengths remained constant while applying tension. After stretching, the knee was brought to the starting position at the "C" point at the 109th second with the movement of the seventh linear actuator and then the parallel robot until 72 seconds and stopped the movement. The second volunteer performed

the knee extension active exercise between 2.5 and 32 seconds and stopped the movement at the "D" point at 42°. Between the 32nd and 35th seconds, the robot switched to the assisted mode because the movement did not continue and the force value decreased. The array brought it to 89.9° ROM at point "E" at 58 seconds, while the piston lengths remained constant while applying the stretch. After stretching, the knee was brought to the starting position at the "F" point at the 98th second with the movement of the seventh linear actuator and then the parallel robot until the 74th second and stopped the movement. Force/torque sensor data for the two volunteers during this time are shown in Fig. 19e and h, respectively. In this motion, linear force sensing in the *y*- and *z*-axis of the 6-axis force/torque sensor and torque sensing in the *x*-axis are used for position-based impedance control of the parallel robot.

The force value for the position-based impedance control of the seventh linear actuator is obtained from the linear force variation in the *y*-axis direction of the 6-axis force/torque sensor. At points "A" and "D" in the graphs, the changes in the force/torque sensor are shown while the volunteers are actively exercising. After the first volunteer made the extension movement actively up to the "A" point, the robot continued its movement at this point when the force values in the *y*- and *z*-axis decreased to zero or below. After the second volunteer made the extension movement actively up to the "D" point, the robot movement continued at this point as the force values in the *y*- and *z*-axis first decreased and then decreased to zero and below.

6. CONCLUSION AND OUTLOOK

The ability of a newly developed rehabilitation robot to perform active and active-assisted ROM recovery exercises was tested on healthy volunteers. The active rehabilitation exercises have been performed with position-based impedance control method on a male and a female healthy volunteer with different leg lengths and weights. A mathematical infrastructure and software have been designed according to the rehabilitation application by selecting the desired ROM of the patient's lower limb. The measurment have yıelded that position accuracy in the linear actuators used ın the robotıc confıguratıon can operate wıth a quıte neglıble devıatıon of lower than 1%. The torque differences applied by two volunteers with different characteristics did not exceed ±0.8 Nm, whıle the force differences resulted lower values than ±2 N. According to the applied force and torque, a proportional increase in the piston speeds of the robot was observed. It has been recorded that in the active assisted exercise mode, the system can seamlessly transist from position-based impedance control mode to PID position control mode by sensing the change in force. The robot transitioned to the PID-controlled position mode with the force or torque occurring in the “0” and/or reverse direction, and the limb could be brought to the standard ROM values with a maximum deviation of 1.3%. Futhermore, it has been evaluated that the speed of the movement increases in direct proportion to the torque. As a result, it has been verified by experiments that the robot can perform the desired movement in relation to the force with high precision, accuracy and repeatability. As a result, experiments on healthy individuals have shown that the robot can perform active and actively assisted rehabilitation exercises in accordance with standard ROMs. For the future, it is targetted that studies on strengthening exercises (isometric, isotonic, isokinetic) and walking exercises can be carried out with a combination of interactively created lower limb rehabilitation robot and EMG signals to be taken from the relevant muscles of the leg. In addition, it is foreseen that this prototype robot, which has been patented, can be brought to hospitals and rehabilitation centers by industrial design and reducing production costs in order to serve more patients and to reduce occupational deformations of physiotherapists.

Acknowledgment

This study was supported by the projects numbered 2018BM0040 and 2021BM02 of the Scientific Research Project Coordinatorship of the Turkish-German University, Istanbul, Turkiye, and. was approved to conduct human experiments with the approval of Koc University Ethics Committees numbered 2020.059.IRB2.018.

REFERENCES

Alwan, H. M., & Sarhan, R. A. (2019). Kinematics Simulation of Gough-Stewart Parallel Manipulator by Using Simulink Package in Matlab Software. *Journal of University of Babylon for Engineering Sciences*, *27*(2), 10–20. https://doi.org/10.29196/jubes.v27i2.2289

Ayas, M. S., & Altas, I. H. (2018). Designing and implementing a plug-in type repetitive controller for a redundantly actuated ankle rehabilitation robot. *Proceedings of the Institution of Mechanical Engineers. Part I: Journal of Systems and Control Engineering*, *232*(5), 592–607. https://doi.org/10.1177/0959651818762062

Ayas, M. S., Altas, I. H., & Sahin, E. (2018). Fractional order based trajectory tracking control of an ankle rehabilitation robot. *Transactions of the Institute of Measurement and Control*, *40*(2), 550–564. https://doi.org/10.1177/0142331216667810

Ba, K. X., Yu, B., Ma, G., Zhu, Q., Gao, Z., & Kong, X. (2018). A Novel Position-Based Impedance Control Method for Bionic Legged Robots' HDU. *IEEE Access*, *6*, 55680–55692. https://doi.org/10.1109/ACCESS.2018.2871244

Budaklı, M. T., & Yılmaz, C. (2021). Stewart platform based robot design and control for passive exercises in ankle and knee rehabilitation. *Journal of the Faculty of Engineering and Architecture of Gazi University*, *36*(4), 1831–1846. https://doi.org/10.17341/gazimmfd.846641

Chisholm, K. J., Klumper, K., Mullins, A., & Ahmadi, M. (2014). A task oriented haptic gait rehabilitation robot. *Mechatronics*, *24*(8), 1083–1091. https://doi.org/10.1016/j.mechatronics.2014.07.001

Díaz, I., Gil, J. J., & Sánchez, E. (2011). Lower-Limb Robotic Rehabilitation: Literature Review and Challenges. *Journal of Robotics*, *2011*(i), 1–11. https://doi.org/10.1155/2011/759764

Dong, F., Li, H., & Feng, Y. (2022). Mechanism Design and Performance Analysis of a Sitting/Lying Lower Limb Rehabilitation Robot. *Machines*, *10*(8), 674. https://doi.org/10.3390/machines10080674

Dong, M., Zhou, Y., Li, J., Rong, X., Fan, W., Zhou, X., & Kong, Y. (2021). State of the art in parallel ankle rehabilitation robot: a systematic review. *Journal of NeuroEngineering and Rehabilitation*, *18*(1), 1–15. https://doi.org/10.1186/s12984-021-00845-z

Eckhoff, D., Hogan, C., DiMatteo, L., Robinson, M., & Bach, J. (2007). An ABJS best paper: Difference between the epicondylar and cylindrical axis of the knee. *Clinical Orthopaedics and Related Research*, *461*, 238–244. https://doi.org/10.1097/BLO.0b013e318112416b

Esmer, A. F., Başarır, K., & Binnet, M. (2011). Diz ekleminin cerrahi anatomisi Surgical anatomy of knee joint. *TOTBİD Dergisi*, *10*(1), 38–44.

Feng, Y., Wang, H., Lu, T., Vladareanuv, V., Li, Q., & Zhao, C. (2016). Teaching Training Method of a Lower Limb Rehabilitation Robot. *International Journal of Advanced Robotic Systems*, *13*(2), 57. https://doi.org/10.5772/62445

Girone, M., Burdea, G., Bouzit, M., Popescu, V., & Deutsch, J. E. (2001). Stewart platform-based system for ankle telerehabilitation. *Autonomous Robots*, *10*(2), 203–212. https://doi.org/10.1023/A:1008938121020

Girone, M. J., Burdea, G. C., & Bouzit, M. (1999). "Rutgers ankle" orthopedic rehabilitation interface. *American Society of Mechanical Engineers, Dynamic Systems and Control Division (Publication) DSC*, *67*, 305–312.

Jamwal, P. K., & Hussain, S. (2016). Design optimization of a cable actuated parallel ankle rehabilitation robot: A fuzzy based multi-objective evolutionary approach. *Journal of Intelligent and Fuzzy Systems*, *31*(3), 1897–1908. https://doi.org/10.3233/JIFS-16030

Kizir, S., & Bingül, Z. (2014). Fuzzy impedance and force control of a Stewart platform. *Turkish Journal of Electrical Engineering and Computer Sciences*, *22*(4), 924–939. https://doi.org/10.3906/elk-1208-54

Liu, G., Gao, J., Yue, H., Zhang, X., & Lu, G. (2006). Design and Kinematics Analysis of Parallel Robots for Ankle Rehabilitation. *2006 IEEE/RSJ International Conference on Intelligent Robots and Systems*, *1*, 253–258. https://doi.org/10.1109/IROS.2006.281710

Mohanta, J. K., Mohan, S., Deepasundar, P., & Kiruba-Shankar, R. (2018). Development and control of a new sitting-type lower limb rehabilitation robot. *Computers & Electrical Engineering*, *67*, 330–347. https://doi.org/10.1016/j.compeleceng.2017.09.015

Peng, L., Hou, Z. G., Peng, L., & Wang, W. Q. (2016). Experimental study of robot-Assisted exercise training for knee rehabilitation based on a practical EMG-driven model. *Proceedings of the IEEE RAS and EMBS International Conference on Biomedical Robotics and Biomechatronics*, *2016-July*, 810–814. https://doi.org/10.1109/BIOROB.2016.7523727

Rakhodaei, H., Saadat, M., Rastegarpanah, A., & Abdullah, C. Z. (2016). Path planning of the hybrid parallel robot for ankle rehabilitation. *Robotica*, *34*(1), 173–184. https://doi.org/10.1017/S0263574714001210

Sarhan, R., & Alwan, H. M. (2019). *Singularity Free Positioning of Gough Stewart Robot Platform* (Issue May). https://doi.org/10.13140/RG.2.2.24181.73442

Shen, Z., Zhuang, Y., Zhou, J., Gao, J., & Song, R. (2020). Design and Test of Admittance Control with Inner Adaptive Robust Position Control for a Lower Limb Rehabilitation Robot. *International Journal of Control, Automation and Systems*, *18*(1), 134–142. https://doi.org/10.1007/s12555-018-0477-z

Song, P., Yu, Y., & Zhang, X. (2017). Impedance Control of Robots: An Overview. *2017 2nd International Conference on Cybernetics, Robotics and Control (CRC)*, *2018-Janua*(1), 51–55. https://doi.org/10.1109/CRC.2017.20

Tsoi, Y. H., & Xie, S. Q. (2008). Design and control of a parallel robot for ankle rehabilitation. *15th International Conference on Mechatronics and Machine Vision in Practice, M2VIP'08*, 515–520. https://doi.org/10.1109/MMVIP.2008.4749585

Wang, C., Fang, Y., Guo, S., & Chen, Y. (2013). Design and kinematical performance analysis of a 3-RUS/RRR redundantly actuated parallel mechanism for ankle rehabilitation. *Journal of Mechanisms and Robotics*, *5*(4). https://doi.org/10.1115/1.4024736

Wang, D., Li, J., & Li, C. (2009). An adaptive haptic interaction architecture for knee rehabilitation robot. *2009 International Conference on Mechatronics and Automation*, 84–89.

https://doi.org/10.1109/ICMA.2009.5246430

Yoshikawa, T. (2000). Force control of robot manipulators. *In Proceedings 2000 ICRA. Millennium Conference. IEEE International Conference on Robotics and Automation.*, *1*, 220–226. https://doi.org/10.1080/00207179008953523